

COMBINED USE OF AN INSTABILITY INDEX AND SEVIRI WATER VAPOR IMAGERY TO DETECT UNSTABLE AIR MASSES

Stavros Kolios^{1,2}, Chrysostomos Stylios¹

¹Laboratory of Knowledge and Intelligent Computing (KIC-LAB), Technological and Educational Institute of Epirus, Arta, Greece.

²Open University of Cyprus, Faculty of Pure and Applied Sciences

ABSTRACT

Nowcasting procedures about the convection and its extreme weather consequences are based on the detection of unstable air masses in order to provide timely and accurate results. In this study, instability indices and MSG derived Brightness Temperatures (BT) are combined to identify suitable thresholds for potentially unstable air masses detection and consequently possible convective cloud regions in early stages of their development. After the spatio-temporal correlation of SEVIRI images and radiosonde data, a statistical analysis is conducted to define the best statistical scores. For the period and area of study, there were found in total 221 different radiosonde profiles with valid measurements in all the measured atmospheric levels. Considering that KI values above a threshold define unstable air masses, there were tested different threshold values and the best statistical scores identified the K.I value equal (or above) to 20°C, the BT of channel 6.2 μm equal (or below) to 240 K and the D_{BT} of channels 6.2 μm and 7.3 μm ($BT_{6.2\mu\text{m}} - BT_{7.3\mu\text{m}}$) equal (or above) to -20 K (F.A.R = 10.19%, P.O.D = 77.9%, Acc. = 74.66%). The accuracy of the proposed threshold combination of the SEVIRI Brightness Temperatures in the water vapor region to discriminate atmospheric instability was evaluated using 3-hourly TRMM satellite accumulated precipitation product. Our study proved that the proposed channels along with the identified threshold values can be applied in operational applications using MSG imagery to delineate unstable air masses (and consequently possible convective areas) even if there is lack of additional data in (near) real-time basis like lightning and/or radiosonde measurements.

INTRODUCTION

The Mediterranean basin has complex geographic features including orography, large coastline, numerous islands and therefore important sea - land interactions. Additionally, the increasing population (mainly in the coastal areas) and the human induced activities cause significant changes that affect in the natural environment. Considering also the influence from both subtropical and mid-latitude atmospheric circulations (Trigo *et al.*, Alpert *et al.*, 2006), the Mediterranean basin can be said that has a sensitive climatic profile. Furthermore the climatic variations affect the intensity and the frequency of occurrence of severe weather situations. Nowadays, there is an increasing use of Meteosat satellite series to monitor effectively severe weather phenomena and many applications are already using the provided information of Meteosat for monitoring and short range forecast purposes (e.g. Puca *et al.*, 2005; Morel and Senesi 2002; Kolios and Feidas 2012; Rigo *et al.*, 2010). Nevertheless, the complex nature of the severe weather phenomena and their rapid evolution in time and space deteriorates the capability of a satellite based application to estimate accurately and timely the evolution of extreme weather events. It is essential in all nowcasting procedures, a timely and accurate detection of all unstable air masses in order to achieve the best results about the convection and its extreme weather consequences (e.g. Marinaki *et al.*, 2006; Merk and Zinner, 2013). In the field of identifying pre-convective atmospheric events, the two available

water vapor channels of Meteosat Second Generation are a valuable tool (e.g. Georgiev and Santurrett, 2009).

The aim of this study is to propose a combination of instability indices and SEVIRI derived Brightness Temperatures (BT) in Water Vapor (WV) so that to identify the most suitable isotherms and the corresponding thresholds of potentially unstable air masses that can lead to early detection of possible convective clouds.

DATA AND METHODOLOGY

For the scope of the study, two kinds of datasets are used. Firstly, radiosonde profiles for the greater area of Mediterranean basin corresponding collected for a two-day period (5/6/2008 - 6/6/2008). The exact locations of the radiosondes are seen in Figure 1. The radiosonde datasets are provided from the National Oceanic and Atmospheric Administration (NOAA) of the United States of America.

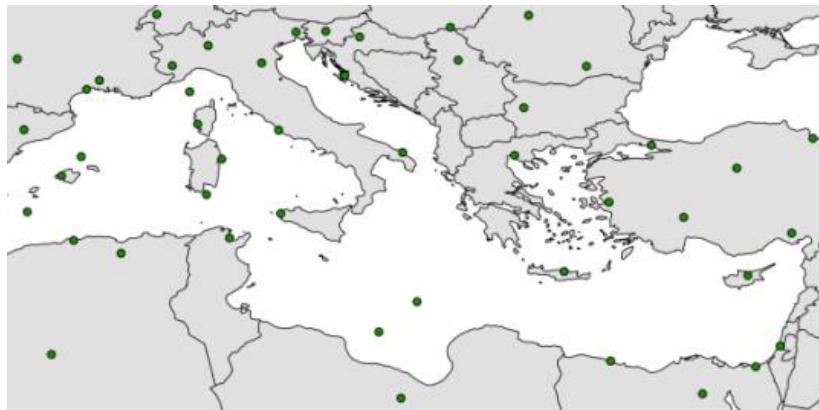


Figure 1: The radiosonde locations used in the study. In the same location may exist different radiosonde profiles as they are released daily at different times.

For all the available data from radiosondes there were finally used only those that they had valid values in all the measured atmospheric levels and at least three consecutive measurements with Relative Humidity (RH) equal or above to 85% with no other measurement of RH above this threshold in the same radiosonde. This RH criterion is used to ensure that the radiosonde refers to cloudy situations. The above mentioned criteria are met by 221 different valid radiosonde profiles. Equation (1) is used to calculate the K-index (K.I) for each of the valid radiosonde profiles.

$$K.I = (T_{850hPa} - T_{850hPa}) + Td_{850hPa} - (T_{700hPa} - Td_{700hPa}) \quad (1)$$

Where T_{850hPa} and T_{700hPa} Are the temperature values at 850hPa and 700hPa respectively, and $T_{d850hPa}$ and $T_{d700hPa}$ are the dew point temperatures at the same pressure heights.

Regarding Meteosat images, there are selected the water vapor channels (channels 6.2 μm , and 7.3 μm) of the SEVIRI instrument in 15-min timesteps during the whole two-day period.

The initial data files converted into Brightness Temperatures and the temperature differences D_{BT} ($BT_{6.2\mu m} - BT_{7.3\mu m}$) in pixel basis, calculated.

Then a spatiotemporal correlation conducted for the two datasets. More analytically, at any time there is a radiosonde with valid measurements (in all the measured heights), a 3 x 3 "window" of the corresponding SEVIRI images is designed, having as center the location of the radiosonde release (Figure 2). As a result, for every radiosonde profile, all the SEVIRI BT and D_{BT} pixel values in the 3 x 3 "window" around the initial location of the radiosonde, in a three-hour period starting from the exact time that the radiosonde was released, are correlated with the values and the K.I of the specific radiosonde profile.

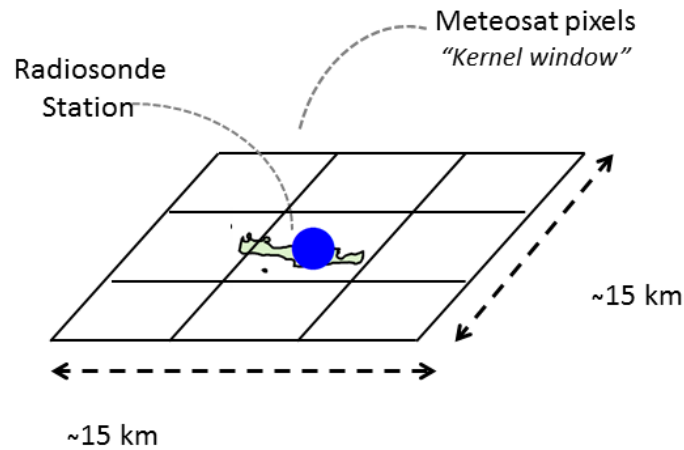


Figure 2: Schematic example of spatial correlation between radiosonde and Meteosat pixels.

RESULTS

After the spatiotemporal correlation between radiosonde measurements and WV SEVIRI imagery, the corresponding contingency tables created and three statistical scores (F.A.R, P.O.D and Accuracy) calculated in order to identify the most suitable thresholding combination among K.I, BT and D_{BT} . The general concept of these contingency tables is presented in Table 1.

	Unstable air masses	Stable air masses
K.I \geq threshold	a	b
K.I < threshold	c	d

Table 1: General criteria scheme to detect combinations for unstable air masses discrimination.

$$F.A.R = \frac{b}{a+b} \cdot 100 \% \text{ (False Alarm Ratio)} \quad (1)$$

$$P.O.D = \frac{a}{a+c} \cdot 100 \% \text{ (Probability of Detection)} \quad (2)$$

$$Accuracy = \frac{a+d}{a+b+c+d} \cdot 100 \% \quad (3)$$

The different thresholds used to define “unstable air masses” and “stable air masses” as well the K.I threshold are presented in Table 2 along with the relative statistical score values. The best threshold combination is achieved for K.I at 20°C, $BT_{6.2\mu m} \leq 240K$ and $BT_{6.2\mu m-7.3\mu m} \geq -20K$. It is mentioned that similar K.I threshold values were also found in other studies (e.g Haklander and Van Delden, 2003).

The 90-min time-lag after the released time of a radiosonde, is considered as a satisfactory period until a radiosonde to reach the upper layers of the troposphere, where it records the atmospheric variables of interest. Figure 3 and Figure 4 present the mean BT and D_{BT} evolution for the “unstable air masses” cases and “stable air masses” cases that they are defined using the best criterion regarding the statistical scores of Table 2.

K.I (°C)	Discrimination of cases		Statistical Score		
	Unstable air masses	Stable air masses	FAR	POD	Acc.
20	$BT_{6.2\mu m} \leq 235K$ AND $DBT_{6.2\mu m-7.3\mu m} \geq -20K$	$BT_{6.2\mu m} > 235K$ OR $DBT_{6.2\mu m-7.3\mu m} < -20K$	30.57	80.1	61.54
	$BT_{6.2\mu m} \leq 240K$ AND $DBT_{6.2\mu m-7.3\mu m} \geq -20K$	$BT_{6.2\mu m} > 240K$ OR $DBT_{6.2\mu m-7.3\mu m} < -20K$	10.19	77.9	74.66
	$BT_{6.2\mu m} \leq 240K$ AND $DBT_{6.2\mu m-7.3\mu m} \geq -15K$	$BT_{6.2\mu m} > 240K$ OR $DBT_{6.2\mu m-7.3\mu m} < -15K$	38.85	76.8	59.27
	$BT_{6.2\mu m} \leq 235K$ AND $DBT_{6.2\mu m-7.3\mu m} \geq -15K$	$BT_{6.2\mu m} > 235K$ OR $DBT_{6.2\mu m-7.3\mu m} < -15K$	47.78	84.5	59.28
	$BT_{6.2\mu m} \leq 235K$ AND $DBT_{6.2\mu m-7.3\mu m} \geq -20K$	$BT_{6.2\mu m} > 235K$ OR $DBT_{6.2\mu m-7.3\mu m} < -20K$	24.6	69.8	67.42
	$BT_{6.2\mu m} \leq 240K$ AND $DBT_{6.2\mu m-7.3\mu m} \geq -20K$	$BT_{6.2\mu m} > 240K$ OR $DBT_{6.2\mu m-7.3\mu m} < -20K$	7.9	63.3	65.16
25	$BT_{6.2\mu m} \leq 240K$ AND $DBT_{6.2\mu m-7.3\mu m} \geq -20K$	$BT_{6.2\mu m} > 240K$ OR $DBT_{6.2\mu m-7.3\mu m} < -20K$	30.95	55.0	87.03
	$BT_{6.2\mu m} \leq 240K$ AND $DBT_{6.2\mu m-7.3\mu m} \geq -15K$	$BT_{6.2\mu m} > 240K$ OR $DBT_{6.2\mu m-7.3\mu m} < -15K$	43.65	86.5	70.14
	$BT_{6.2\mu m} \leq 235K$ AND $DBT_{6.2\mu m-7.3\mu m} \geq -15K$	$BT_{6.2\mu m} > 235K$ OR $DBT_{6.2\mu m-7.3\mu m} < -15K$	3	8	8
	$BT_{6.2\mu m} \leq 235K$ AND $DBT_{6.2\mu m-7.3\mu m} \geq -20K$	$BT_{6.2\mu m} > 235K$ OR $DBT_{6.2\mu m-7.3\mu m} < -20K$	5	5	5
	$BT_{6.2\mu m} \leq 240K$ AND $DBT_{6.2\mu m-7.3\mu m} \geq -15K$	$BT_{6.2\mu m} > 240K$ OR $DBT_{6.2\mu m-7.3\mu m} < -15K$	8	3	3
	$BT_{6.2\mu m} \leq 235K$ AND $DBT_{6.2\mu m-7.3\mu m} \geq -15K$	$BT_{6.2\mu m} > 235K$ OR $DBT_{6.2\mu m-7.3\mu m} < -15K$	8	3	3

Table 2: The values are referred to 90 min after the release time of a radiosonde.

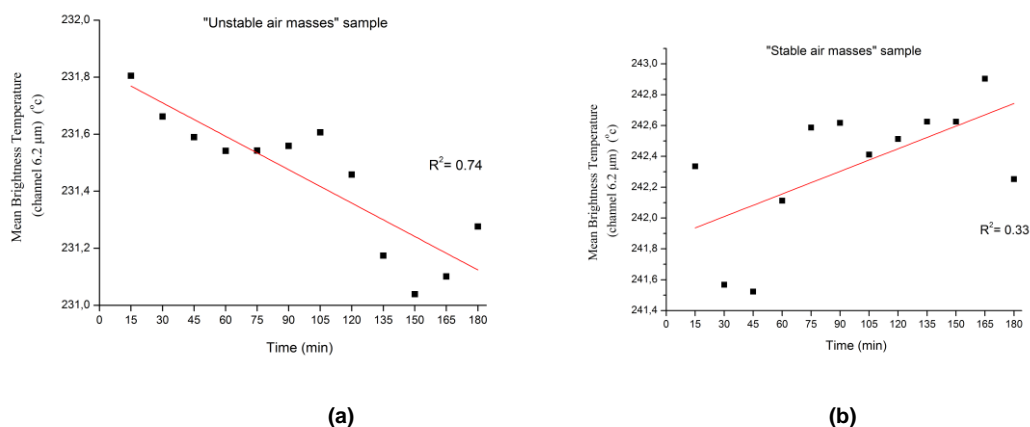


Figure 3: Mean Brightness Temperature for all the pixels included in all 3 x 3 “windows” of the SEVIRI channel of 6.2 μm imagery, centered in the initial location of a radiosonde during a 3-hour period started from the time a radiosonde is released in 15-min timesteps (temporal resolution of SEVIRI imagery). Figure (a) is referred in the “unstable air masses” sample and (b) in the “stable air masses” one.

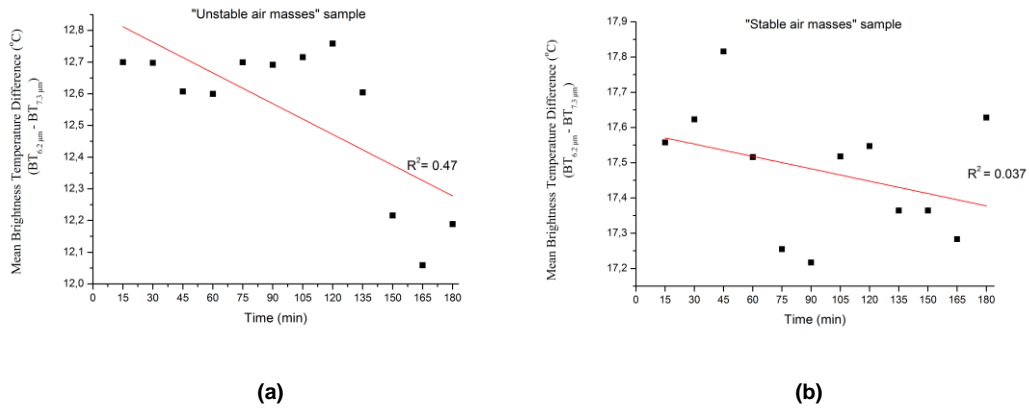


Figure 4: The same as Figure 3 but for the temperature differences D_{BT} ($BT_{6.2\mu m} - BT_{7.3\mu m}$).

Figures 5 and 6 provide characteristic examples of the areas defined by the “unstable air masses” criteria ($BT_{6.2\mu m} \leq 240K$ and $DBT_{6.2\mu m-7.3\mu m} \geq -20K$ according to Table 1).

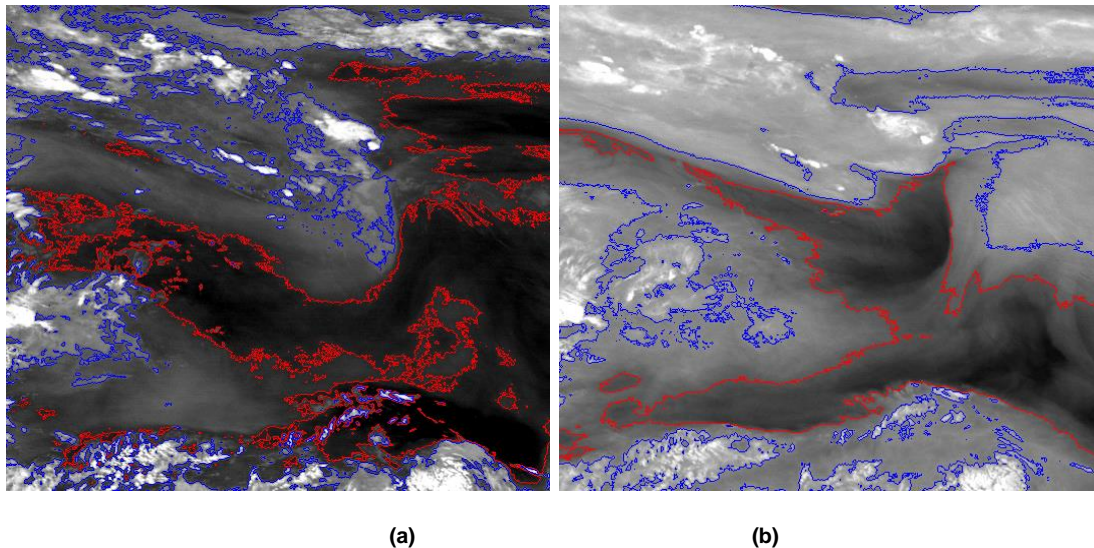


Figure 5: (a) $DBT_{6.2\mu m-7.3\mu m}$ image at 05/06/2008 (00:00 UTC). The red colored contours depict -20K Brightness Temperature Difference and the blue colored contours depict -15K Brightness Temperature Difference, (b) The $BT_{6.2\mu m}$ image at 05/06/2008 (00:00 UTC). The red colored contours define the 240K isotherm and the blue colored one defines the 235K isotherm.

Figure 5a illustrates the $DBT_{6.2\mu m-7.3\mu m}$ image where the -20K isotherm isolates extended cloud regions either with convective cloud patterns and water vapor amounts in high tropospheric levels or with low tropospheric humidity. Only completely dry regions in all the atmospheric levels are excluded from the -20K isotherm. More closely to convective cloud patterns is the -15K isotherm, but in this study, we concern mainly about pre-convective environments. Figure 5b presents the $BT_{6.2\mu m}$ image where the 240K isotherm includes extended cloud regions of high level water vapor as well as all the convective cloud tops.

Figure 6a provides an alternative view of the examined case as it is seen in the channel of $10.8 \mu m$. Conclusively, the combination of -20K threshold (in the $DBT_{6.2\mu m-7.3\mu m}$ image) and the

240K threshold (in the $BT_{6.2\mu m}$ image) can delineate unstable air masses that are potentially evolved in convective areas. A characteristic example of this threshold combination is inferred from Figure 6b, where the brown colored areas fulfill simultaneously the two previously referred criteria.

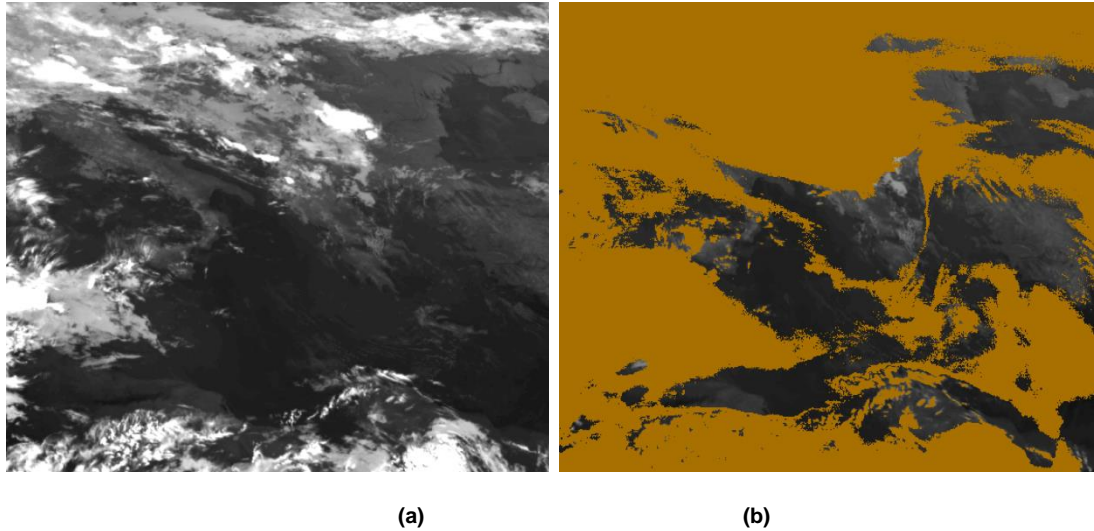


Figure 6: (a) The $10.8 \mu m$ SEVIRI channel image at 05/06/2008 (00:00 UTC). (b) The same image where it is overlaid all the areas (brown colored areas) that fulfill simultaneously the “unstable air masses” criteria ($BT_{6.2\mu m} \leq 240K$ and $DBT_{6.2\mu m-7.3\mu m} \geq -20K$).

VALIDATION

In order to evaluate the accuracy of the proposed criteria combination of SEVIRI $BT_{6.2\mu m}$ and $DBT_{6.2\mu m-7.3\mu m}$ to detect atmospheric instability, we selected all the grid values of TRMM (Huffman *et al.*, 2007) in a 3-hourly accumulated precipitation product (“3B42” product with spatial resolution of $0.25^\circ \times 0.25^\circ$) that correspond to the radiosonde release locations, after a spatiotemporal correlation procedure. Then we split the extracted dataset with the pairs of values (K.I index values and the relative 3-hourly accumulated precipitation) in two different samples: one sample with K.I value lower than $20^\circ C$ and the other with K.I value greater than $20^\circ C$. Finally, we implemented parametric and non-parametric statistical hypothesis tests to evaluate if the mean precipitation for the two different samples differs statistically significantly or not. We conclude that the mean 3-hourly precipitation for the cases where the K.I is above $20^\circ C$ is statistically different than the cases that correspond to K.I values lower than $20^\circ C$.

Samples	Mean precipitation (mm)	Standard deviation (mm)	Hypothesis test (T-test)	Hypothesis test (Mann-Whitney U test)
$K.I \geq 20$	1.14	2.03	p-value = 0.00 at significance level of 0.05	p-value = 0.00 at significance level of 0.05
$K.I < 20$	0.06	0.22		

Table 3: Statistical results of validation procedure of the SEVIRI BT thresholds accuracy in delineating unstable air masses, using 3-hourly TRMM precipitation values.

CONCLUSIONS

In this study we combine SEVIRI water vapor Brightness Temperatures and Temperature Differences ($BT_{6.2\mu m}$ and $DBT_{6.2\mu m-7.3\mu m}$ respectively) with K.I values coming from radiosonde profiles so that to define suitable thresholds for unstable air masses delineation that can potentially lead to convective activity. Our results concluded that the best threshold combination is achieved for K.I at $20^{\circ}C$, $BT_{6.2\mu m} \leq 240K$ and $BT_{6.2\mu m-7.3\mu m} \geq -20K$.

It is also concluded that for the “unstable air masses” sample the $BT_{6.2\mu m}$ and $DBT_{6.2\mu m-7.3\mu m}$ mean “3x3” pixel values of the relative SEVIRI images centered around the release location of every radiosonde, show a decrease larger than 0.5K at the 3-hour duration of each radiosonde.

Figure 5 and Figure 6 shows that it is possible to ascertain the atmospheric areas that are delineated as unstable. It is concluded that the proposed threshold combination includes large atmospheric areas with significant water vapor amounts in the middle and upper troposphere. These areas can contain convective activity areas as it is seen in the isotherm of -15K (Figure 5a) and 235K (Figure 5b).

Finally, we have evaluated the proposed thresholds combination to delineate unstable air masses using a 3-hourly TRMM accumulated precipitation. The validation procedure proved that there is a statistically significant differentiation in the precipitation amounts that correlate spatiotemporally with the radiosonde profiles that have K.I values equal or greater than $20^{\circ}C$ and those that have K.I values smaller than $20^{\circ}C$.

Future work of this study can include a larger amount of datasets, the use of additional instability indices and the examination of different threshold values and SEVIRI channels to improve the accuracy in unstable air masses delineation that is of crucial importance in nowcasting procedures.

ACKNOWLEDGEMENTS

This work is supported by the “Transnational Enhancement of ECOPORT8 network” (TEN ECOPORT) project with code SEE/D/0189/2.2/X, co-financed by the European Union within the South East Europe Transnational Cooperation Programme.

REFERENCES

- Alpert, P., Baldi, M., Ilani, R., Krichak, S., Price, C., Rodó, X., Saaroni, H., Ziv, B., Kishcha, P., Barkan, J., Mariotti, A., Xoplaki, E. Relations between climate variability in the Mediterranean region and the tropics: ENSO, South Asian and African monsoons, hurricanes and Saharan dust, in: Mediterranean Climate Variability. Elsevier B.V., pp. 149–177, 2006.
- George J.J., 1960. Weather Forecasting for Aeronautics, Academic Press, New York, pp. 409-415.
- Georgiev C., Santuret P., 2009. Diagnosis of atmospheric environment favourable for deep moist convection by using satellite imagery. 5th European Conference on Severe Storms, 12 - 16 October 2009 - Landshut – Germany.
- Haklander A.J., Van Delden A., 2003. Thunderstorms predictors and their forecast skill for Netherlands. Atmospheric Research, 67-68, 273-299.

- Huffman, G.J., R.F. Adler, D.T. Bolvin, G. Gu, E.J. Nelkin, K.P. Bowman, Y. Hong, E.F. Stocker, D.B. Wolff, 2007. The TRMM Multi-satellite Precipitation Analysis: Quasi-Global, Multi-Year, Combined-Sensor Precipitation Estimates at Fine Scale. *Journal of Hydrometeorology*, 8, 38-55.
- Kolios, S., Feidas H., 2011. An automated nowcasting system of Mesoscale Convective Systems for the Mediterranean basin using Meteosat imagery. Part I: System description. *Meteorological Applications*, 20 (3), 287-295, DOI: 10.1002/met.1282.
- Marinaki A., Spiliotopoulos M., Michalopoulou H., 2006. Evaluation of atmospheric instability indices in Greece. *Advances in Geosciences*, 7, 131-135.
- Merk D., Zinner T., 2013. Detection of convective initiation using Meteosat SEVIRI: implementation in and verification with the tracking and nowcasting algorithm Cb-TRAM. *Atmospheric Measurement Techniques*, 6, 190-1918.
- Morel C, Senesi S. 2002. A climatology of mesoscale convective systems over Europe using satellite infrared imagery. I: Methodology. *Quarterly Journal of Royal Meteorological Society* 128: 1953-1971.
- Puca S, Biron D, De Leonibus L, Melfi D, Rosci P, Zauli F. 2005. A Neural Network Algorithm for the Nowcasting of Severe Convective Systems. *CIMSA 2005 - IEEE International Conference on Computing Intelligence for Measurement System Applications*. Giardini Naxos, 20-22 July, Italy.
- Rigo T., Pineda N., Bech J., 2010. Analysis of warm season thunderstorms using an object-oriented tracking method based on radar and total lightning data. *Natural Hazards and Earth Systems Sciences*, 10, 1881-1893.
- Trigo, R.M., Xoplaki, E., Luterbacher, J., Krichak, S.O., Alpert, P., Jacobeit, J., Saenz, J., Fernandez, J., Gonzalez-Rouco, J.F. Relations between variability in the Mediterranean region and mid-latitude variability, in: Lionello, P., Malanotte-Rizzoli, P., Boscolo, R. (Eds.), *Mediterranean Climate Variability*. Elsevier, Amsterdam, pp. 179-226, 2006.